AGU PUBLICATIONS

Space Weather

RESEARCH ARTICLE
10.1002/2016SW001494

Key Points:
- Uncertainties propagate in a nonlinear way in radiation belt simulations
- The 2 MeV electron flux can vary by 2 orders of magnitude; this uncertainty must be reduced for forecasting
- Uncertainty in density estimation is the most responsible for variance in output flux

Correspondence to:
E. Camporeale,
e.camporeale@cwi.nl

Citation:
Camporeale, E., Y. Shprits, M. Chandorkar, A. Drozdov, and S. Wing (2016), On the propagation of uncertainties in radiation belt simulations, *Space Weather*, *14*, 982–992, doi:10.1002/2016SW001494.

Received 9 AUG 2016
Accepted 15 OCT 2016
Accepted article online 22 OCT 2016
Published online 5 NOV 2016

On the propagation of uncertainties in radiation belt simulations

Enrico Camporeale[1], Yuri Shprits[2,3], Mandar Chandorkar[1], Alexander Drozdov[3], and Simon Wing[4]

[1]Multiscale Dynamics, Center for Mathematics and Computer Science (CWI), Amsterdam, Netherlands, [2]Helmholtz Centre Potsdam, GFZ German Research Centre for Geosciences, Potsdam, Germany, [3]Department of Earth, Planetary, and Space Sciences, University of California, Los Angeles, California, USA, [4]The Johns Hopkins University Applied Physics Laboratory, Laurel, Maryland, USA

Abstract We present the first study of the uncertainties associated with radiation belt simulations, performed in the standard quasi-linear diffusion framework. In particular, we estimate how uncertainties of some input parameters propagate through the nonlinear simulation, producing a distribution of outputs that can be quite broad. Here we restrict our focus on two-dimensional simulations (in energy and pitch angle space) of parallel-propagating chorus waves only, and we study as stochastic input parameters the geomagnetic index *Kp* (that characterizes the time dependency of an idealized storm), the latitudinal extent of waves, and the average electron density. We employ a collocation method, thus performing an ensemble of simulations. The results of this work point to the necessity of shifting to a probabilistic interpretation of radiation belt simulation results and suggest that an accurate specification of a time-dependent density model is crucial for modeling the radiation environment.

1. Introduction

The temporal evolution of energetic electrons in the Earth's radiation belts is routinely studied via a quasi-linear theory approach, originally introduced by *Kennel and Engelmann* [1966]. The resulting Fokker-Planck equation describes the rate of change of the particle distribution function due to wave-particle interactions and the subsequent violation of one or more of the three adiabatic invariants of motion. The Fokker-Planck equation is generally employed, in radiation belt studies, after averaging out the gyro, bounce, and drift periodic orbits. Hence, it takes the form of a diffusion equation in the adiabatic invariants space. Furthermore, the timescale associated with the third adiabatic invariant (so-called L^*) is well separated from the timescales associated with the first and second invariants. Therefore, it is customary to treat the diffusion in L^* (associated to the radial direction), as nonmixing with diffusion in the first two invariants (associated to energy and pitch angle space). Hence, the Fokker-Planck equation can be written as follows:

$$\frac{\partial f}{\partial t} = \frac{1}{J}\frac{\partial}{\partial L^*}\left(JD_{L^*L^*}\frac{\partial f}{\partial L^*}\right) + \sum_{i,j}\frac{1}{J}\frac{\partial}{\partial x_i}\left(JD_{ij}\frac{\partial f}{\partial x_j}\right), \tag{1}$$

where the coordinates $x_{i,j}$ are related via a change of variables to the two first invariants, and they are usually chosen as energy (or momentum) and equatorial pitch angle. The Jacobian J is calculated accordingly.

The study of equation (1) has represented the focus of much of radiation belt physics research in the past few decades, from both the perspective of developing efficient numerical schemes [*Albert and Young*, 2005; *Xiao et al.*, 2009; *Subbotin and Shprits*, 2012; *Camporeale et al.*, 2013a, 2013b, 2013c; *Albert*, 2013; *Tao et al.*, 2016] and the perspective of understanding the relative importance of different physical mechanisms that contribute to the diffusion coefficients [*Thorne*, 2010; *Tu et al.*, 2014; *Xiao et al.*, 2014; *Jaynes et al.*, 2015]. Indeed, it is important to note that the particle dynamics is entirely determined by the specification of the diffusion coefficients, boundary conditions, and initial conditions, in equation (1). Some of the shortcomings of the quasi-linear diffusion approach have been discussed, for instance, by [*Shalchi and Schlickeiser*, 2005; *Ragot*, 2012; *Lemons*, 2012; *Camporeale and Zimbardo*, 2015; *Camporeale*, 2015].

Several research groups have developed numerical codes to solve the Fokker-Planck equation (1). Some of the most referenced are VERB (Versatile Electron Radiation Belt) [*Shprits et al.*, 2008; *Subbotin and Shprits*, 2009],

Salammbo [*Bourdarie et al.*, 1996; *Bourdarie and Maget*, 2012], STEERB (Storm-Time Evolution of Electron Radiation Belt) [*Xiao et al.*, 2010; *Su et al.*, 2010], the BAS (British Antarctic Survey) code [*Glauert et al.*, 2014], the UCLA-3D code [*Ma et al.*, 2015], and DREAM3D [*Tu et al.*, 2013]. Although some of these groups have also developed an operational infrastructure that allows for real-time forecasts based on simulation outputs (see, e.g., http://rbm.epss.ucla.edu/realtime-forecast/ and http://fp7-spacecast.eu/ [*Horne et al.*, 2013]), most of these studies have mainly focused on understanding the underlying physics. For this reason, these codes are all deterministic; that is, they return a single output, for any specific set of input parameters. A notable exception is the RadBelt Electron Model, recently presented in *Zheng et al.* [2014], that recast the Fokker-Planck equation in terms of stochastic differential equations, hence obtaining a probabilistic distribution of solutions.

In view of the fact that physics-based models are becoming increasingly important in Space Weather [*Tóth et al.*, 2012; *Schunk et al.*, 2016], it is easy to recognize the need for a probabilistic interpretation of simulation outputs, simply because a point estimate is meaningless, without its corresponding confidence interval. In turn, such a probabilistic interpretation requires at least two ingredients: a correct specification of the uncertainties attributed to input parameters and the study of the propagation of such uncertainties through our physics-based model. This paper is concerned with the latter task, that is, the attempt to characterize how an imperfect knowledge of our input parameters is reflected in the simulation output.

As we will discuss in the following, radiation belt simulations are built on a large number of input parameters related to wave spectra, atmospheric and magnetopause losses, and consequently on an equally large number of assumptions regarding such parameters. The common approach is to specify single values for these inputs that have been derived from statistical studies of historical data [*Meredith et al.*, 2003; *Shprits et al.*, 2007; *Agapitov et al.*, 2013; *Meredith et al.*, 2014].

The field of uncertainty quantification (UQ) has witnessed a rapid growth in the last few decades, and it now represents a central topic in engineering research and applications [*Smith*, 2013]. The tools of UQ are still relatively unknown in space physics, although, for instance, the technique of ensemble forecasting has seen some recent advances in space weather [*Knipp*, 2016]. A general classification divides UQ techniques between *nonintrusive* and *intrusive*. The former term refers to using a deterministic model as a black-box simulator that can run multiple times, while the latter is used when the underlying partial differential equations are recast in terms of stochastic equations. We refer to the tutorial by *Xiu* [2009] for a discussion of these and other details of UQ. In this work we employ a nonintrusive approach, performing an ensemble of simulations with the extensively benchmarked VERB code. The probability distribution of the input parameter space is preassigned, and it is explored with a fairly naive version of a collocation algorithm, described in section 2.

This paper represents the first attempt to study the propagation of uncertainties in a radiation belt model. For this reason, we limit our scope to (1) two-dimensional simulations in energy and pitch angle and (2) the study of the following three input parameters only: the geomagnetic index *Kp*, the maximum latitude extent of wave propagation $\lambda_{\max}$, and the average electron number density n.

The paper is organized as follows. Section 2 presents the methodology, including the details of the simulation setup, and the assumed distribution of the input parameters. Results are discussed in section 3, where we will analyze the relative importance of each of the input parameters under consideration. Finally, conclusions and future research directions are drawn in section 4.

2. Methodology

We have employed the two-dimensional version of the VERB code, to solve diffusion in energy and pitch angle, and we have performed an ensemble of simulations, each one with different input parameters, and a given probability of occurrence. We have neglected cross-diffusion, for computational saving. Although it is now understood that the electron phase space density might be overestimated, especially at high energy, we believe that the results presented in the following are still relevant, for what concerns the propagation of uncertainties.

The numerical grid has 201 points in each direction, with energy E ranging from 0.2 to 5 MeV and equatorial pitch angle α ranging from 5° to 89.7°. L^* is kept fixed at a value of 4.5. The initial condition for the particle distribution function is the same used in *Albert et al.* [2016], and it is chosen as $f = j/p^2$, with the flux

$$j = j_0 e^{-E/E_0} \left(\sin\alpha - \sin\alpha_{\mathrm{LC}}\right), \tag{2}$$

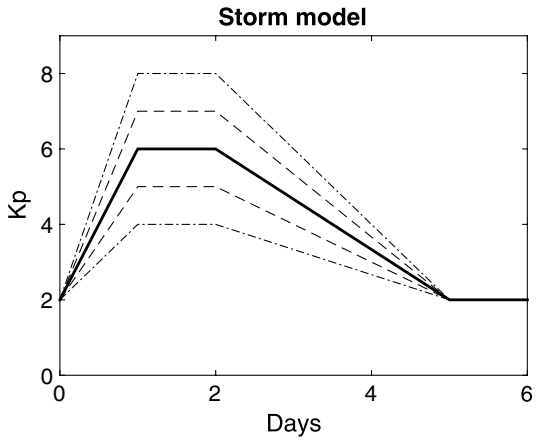

Figure 1. Geomagnetic index *Kp* for the idealized storm used in this study. Solid, dashed, and dash-dotted lines correspond to different unnormalized probabilities of 1, $e^{-1/2}$, and e^{-2}, respectively.

where p is momentum, α_{LC} is the loss cone value of α in a dipole, and $j_0 = 2.5 \times 10^5$ cm^{-2} s^{-1} sr^{-1} keV^{-1}. The boundary conditions are also standard: $f = 0$ for $\alpha = \alpha_{LC}$, $\partial f/\partial\alpha = 0$ for $\alpha = 89.7$, and f is kept constant at the lower and higher energy boundaries.

For simplicity, the simulations include chorus day and night parallel-propagating waves only, with the same parameters as in *Shprits et al.* [2009]. In principle, the calculation of the diffusion coefficients needs to specify the average wave amplitude (and its parametrization as a function of *Kp*), the wave spectral properties (that is, assuming a Gaussian distribution in frequencies, the upper and lower limits, and mean and bandwidth frequencies), the percentage MLT (Magnetic Local Time) coverage, the electron density n, the maximum latitudinal extent of the waves λ_{max}, and the time evolution of the geomagnetic index *Kp*. In the present approach each of these quantities might be treated as a random variable. In this paper, however, we focus on the last three quantities only (n, λ_{max}, and *Kp*).

We study the effect of input parameter uncertainties on an idealized storm, previously studied in *Shprits et al.* [2009]. The storm model is parametrized solely by the geomagnetic index *Kp*, as depicted in Figure 1. We assume that at initial time (day = 0) $Kp = 2$, it grows linearly within the first day, it stays at a constant level until day 2, and it finally decreases linearly reaching its starting value at day 5. The *Kp* evolution represented by solid, dashed, and dash-dotted lines correspond to different maximum values of *Kp* achieved during day 1 and to unnormalized probabilities of 1, $e^{-1/2}$, and e^{-2}, respectively.

The three input parameters *Kp*, λ_{max}, and n are assumed to be independently distributed according to a Gaussian. Figure 2 shows their (unnormalized) probabilities. The values that are chosen to form the simulation ensemble are shown as black squares. It is understood that the probability attributed to a single simulation is the product of the probabilities attributed to the chosen values of *Kp*, λ_{max}, and n, appropriately normalized. Hence, the input space is modeled as a multivariate (three-dimensional) Gaussian distribution, which is explored on a fixed three-dimensional grid of $5 \times 5 \times 9 = 225$ points in the *Kp*, λ_{max}, and n directions. Figure 2 (left) is the maximum value of *Kp* of the idealized storm shown in Figure 1, that is, the value reached between days 1 and 2. The values for its mean and the standard deviation are equal to 6 and 1, respectively. The five points chosen for sampling are $Kp = \{4, 5, 6, 7, 8\}$, with corresponding unnormalized probabilities equal to $\{e^{-2}, e^{-1/2}, 1, e^{-1/2}, e^{-2}\}$. Figure 2 (middle) shows the distribution of the maximal latitudinal extent of the chorus day (blue) and chorus night (red) waves. We assume that the two kinds of waves are completely correlated;

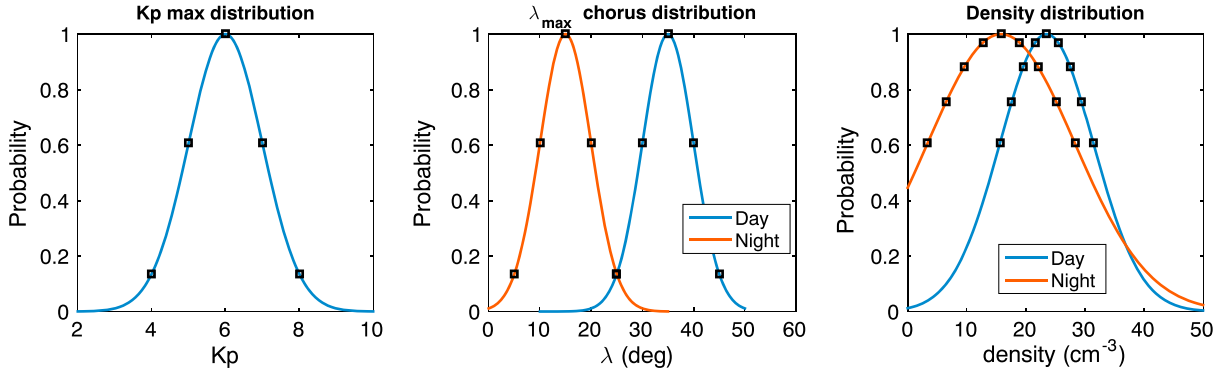

Figure 2. Distribution of input parameters. (left) Maximum value of the *Kp* index (achieved during day 1). (center) Maximum latitudinal extent of waves λ_{max} (blue for chorus day and red for chorus night). (right) Electron density distribution (blue for chorus day and red for chorus night). Each distribution is Gaussian, and the three parameters are assumed to be independent. The values chosen for the ensemble of simulations (225 in total) are denoted with squares.

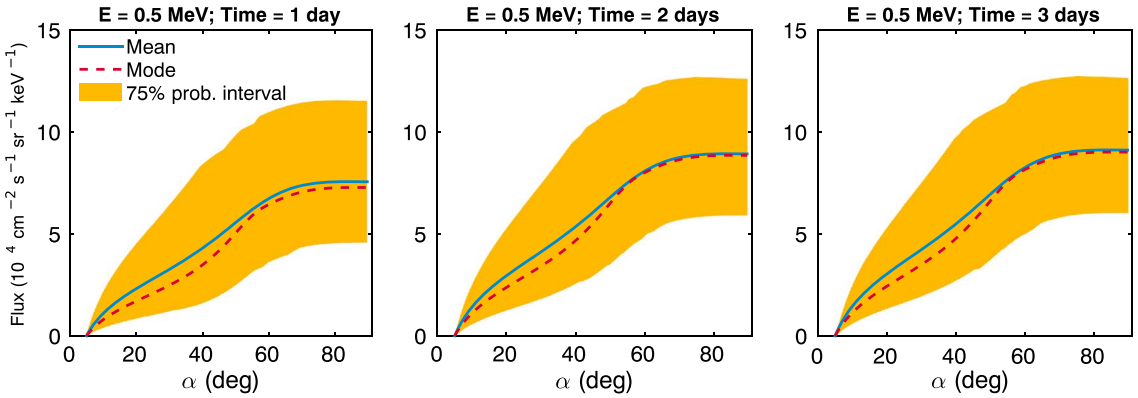

Figure 3. Electron flux (in 10^4 cm^{-2} s^{-1} sr^{-1} keV^{-1}) as a function of pitch angle α for energy equal to 500 keV. (left, middle, and right) The evolution at times 1, 2, and 3 days. The blue line is the mean calculated over the whole ensemble. The dashed red line is the single simulation corresponding to the most probable inputs, and the yellow area covers a region of the flux corresponding to a probability of 75%.

that is, sampling points in the two distributions correspond one to one. The mean values are equal to 35° and 15° for day and night respectively, and the standard deviation is equal to 5° in both cases. As for the distribution in *Kp* we choose five points: the mean, $\pm\sigma$, and $\pm 2\sigma$ (with σ the standard deviation). This corresponds to $\lambda_{\max}(\text{day}) = \{25, 30, 35, 40, 45\}$ and $\lambda_{\max}(\text{night}) = \{5, 10, 15, 20, 25\}$ (in degrees). Finally, Figure 2 (right) shows the distribution of the electron density, which has been calculated following the estimation in *Sheeley et al.* [2001] (equation (7) in that paper, assuming $L = 4.5$, LT = 3 for the chorus night and LT = 9 for the chorus day). In this case the distribution is sampled with nine points separated by a quarter of a standard deviation. In principle, one might use different models for the electron density estimation [see, e.g., *Gallagher et al.*, 2000; *Huang et al.*, 2004]. However, the *Sheeley et al.* [2001] model is particularly suited for this problem, because it provides an analytical formula for the mean and the standard deviation, as functions of *L* and magnetic local time.

We have validated our findings using a smaller ensemble with five points only in the density and checking that the results do not change significantly. We also note that in this restricted three-dimensional parameter space, the sampling method chosen with 225 simulations is already effective; however, one should use more sophisticated methods, such as quasi-Monte Carlo sampling [*L'Ecuyer and Owen*, 2009] or grid-free adaptive stochastic methods, when moving to higher dimensions (including more input parameters).

3. Results

In this section we discuss the results obtained by analyzing the ensemble of simulations, in terms of the statistics of the simulated electron flux, and how this is affected by changing the input parameters. Figures 3 and 4

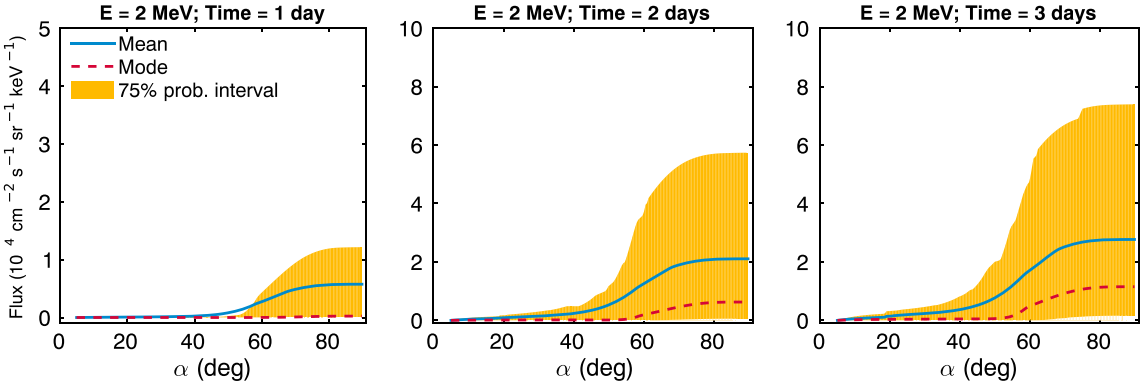

Figure 4. Electron flux (in 10^4 cm^{-2} s^{-1} sr^{-1} keV^{-1}) as a function of pitch angle α for energy equal to 2 MeV. (left, middle, and right) The evolution at times 1, 2, and 3 days. The blue line is the mean calculated over the whole ensemble. The dashed red line is the single simulation corresponding to the most probable inputs, and the yellow area covers a region of the flux corresponding to a probability of 75%.

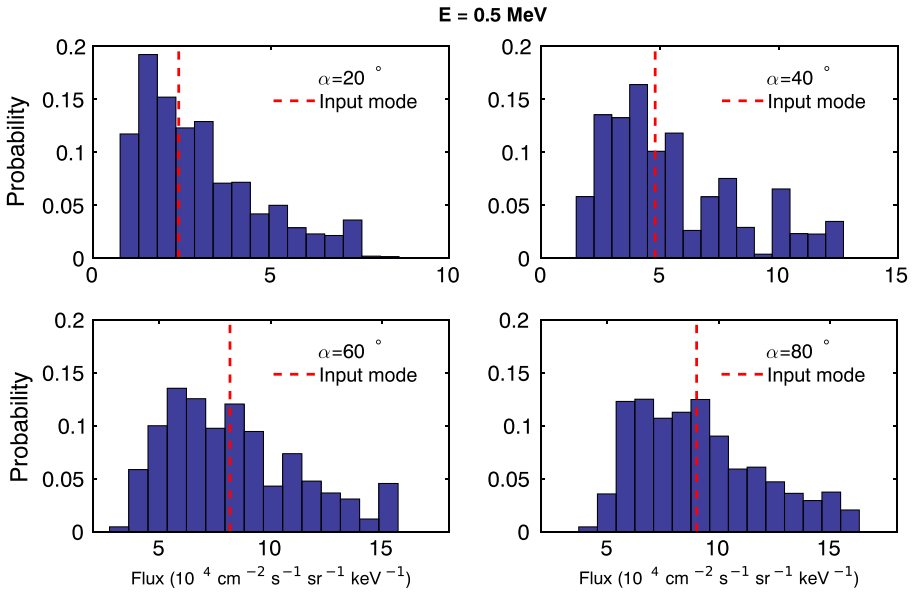

Figure 5. Histograms of electron flux , at time = 3 days, for energy equal to 500 keV. The four panels denote pitch angle α = 20°, 40°, 60°, and 80°. The dashed red line represents the single simulation corresponding to the most probable inputs.

show the flux as a function of pitch angle α, for 500 keV and 2 MeV electrons, respectively. Figures 3 (left, middle, and right) and 4 (left, middle, and right) denote the results after 1, 2, and 3 days. In both figures, the blue line represents the mean value (averaged over the whole ensemble of 225 simulations), the dashed red line shows the result of the single simulation with the highest probability of the inputs (i.e., the mode of the input distribution), and the yellow area bounds the interval containing a simulation result with a probability of 75%. This has been determined by calculating the empirical cumulative distribution of the fluxes (taking into account that each member of the ensemble is associated with an input probability) and denoting as the lower

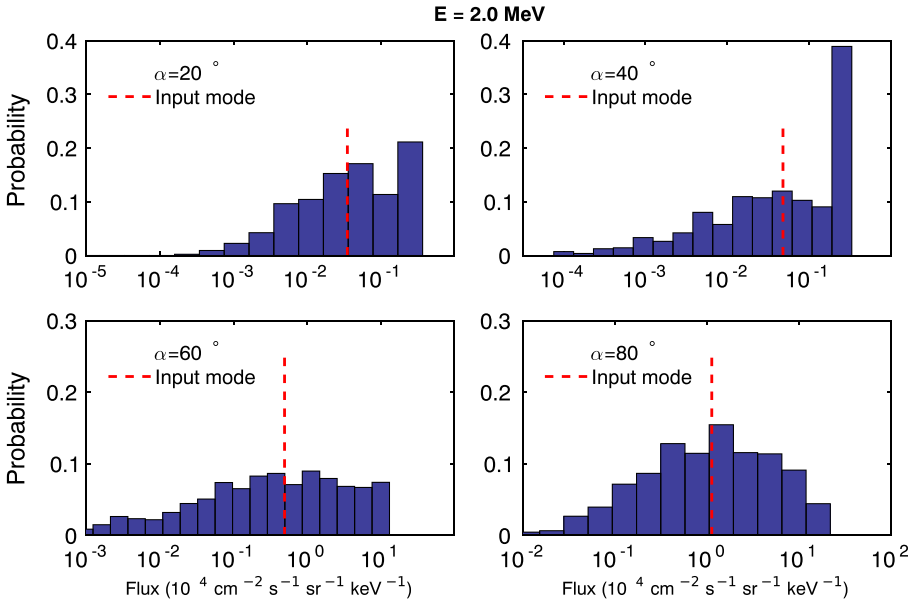

Figure 6. Histograms of electron flux , at time = 3 days, for energy equal to 2 MeV. The four panels denote pitch angle α = 20°, 40°, 60°, and 80°. The dashed red line represents the single simulation corresponding to the most probable inputs.

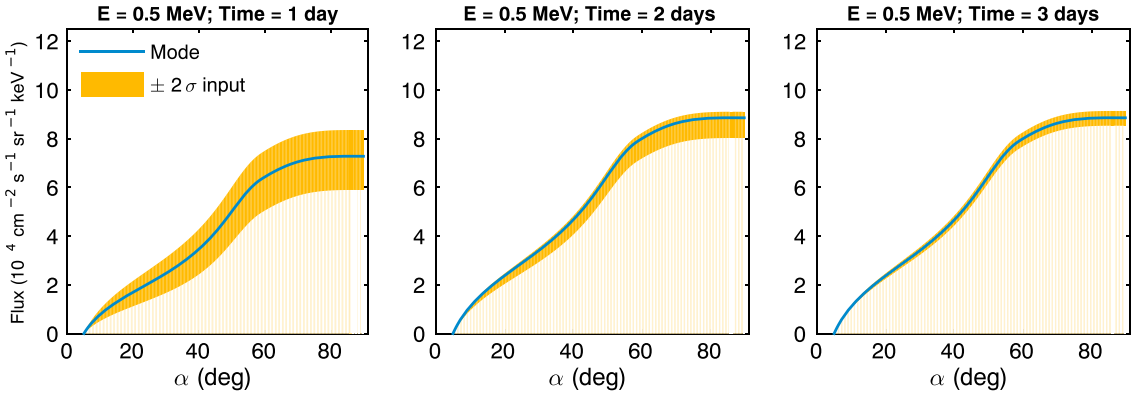

Figure 7. Sensitivity study varying only *Kp*. Electron flux (in 10^4 cm^{-2} s^{-1} sr^{-1} keV^{-1}) as a function of pitch angle α for energy equal to 500 keV. (left, middle, and right) The evolution at times 1, 2, and 3 days. The blue line is the single simulation corresponding to the most probable inputs. The yellow area denotes the extreme values considered in the input distribution ($\pm 2\sigma$).

and higher bounds the values for which such a cumulative distribution is equal to 0.125 and 0.875, respectively. In other words, the probability that a result belongs to the yellow area is 75%. Note that the boundary condition on the loss cone angle (on the left) is of Dirichlet type, imposing the flux to be null. Hence, all the simulations give the same result. On the other hand, the boundary condition for $\alpha = 90°$ is of Neumann type, imposing that the first derivative of the flux vanishes. Consequently, the variance in the flux increases moving to larger angles. Two important results can be discussed. The first is how incorrect it may be to consider only the simulation that carries the highest input probability (the one denoted as the mode in the plots), neglecting the fact that the input parameters should be more properly represented as random variables. In other words, how incorrect is it to neglect the stochastic nature of the system? This question can be answered by looking at the difference between the red and blue lines. The difference is quite small for 500 keV particles, but it becomes nonnegligible for 2 MeV, particularly at large pitch angles (almost a factor of 2). A second point concerns the overall nonlinearity of the system and the associated skewness of the distribution that determines the error bar. While for 500 keV electrons (Figure 3), the mean divides almost equally the shaded yellow area, a clear asymmetry of the distribution is visible for 2 MeV electrons (Figure 4). It is an effect of nonlinearity that a symmetric (Gaussian) input distribution generates a skewed output distribution. In order to better appreciate the distribution of fluxes, we plot in Figures 5 and 6 the histograms for electrons with 500 keV and 2 MeV, respectively, at time = 3 days. The four different panels are for pitch angles $\alpha = 20°, 40°, 60°$, and $80°$. The red dashed line denotes the result of the simulation representing the mode of the input distribution (the one with highest probability). In most cases, the outcome of this single simulation does not agree with the most probable output flux. Moreover, noting that the horizontal axis in Figure 6 is in logarithmic scale,

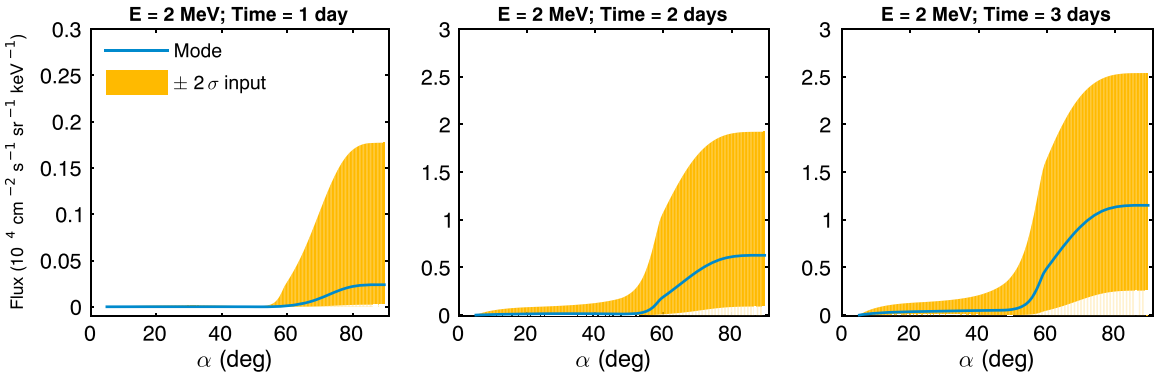

Figure 8. Sensitivity study varying only *Kp*. Electron flux (in 10^4 cm^{-2} s^{-1} sr^{-1} keV^{-1}) as a function of pitch angle α for energy equal to 2 MeV. The three panels show the evolution at times 1, 2, and 3 days. The blue line is the single simulation corresponding to the most probable inputs. The yellow area denotes the extreme values considered in the input distribution ($\pm 2\sigma$).

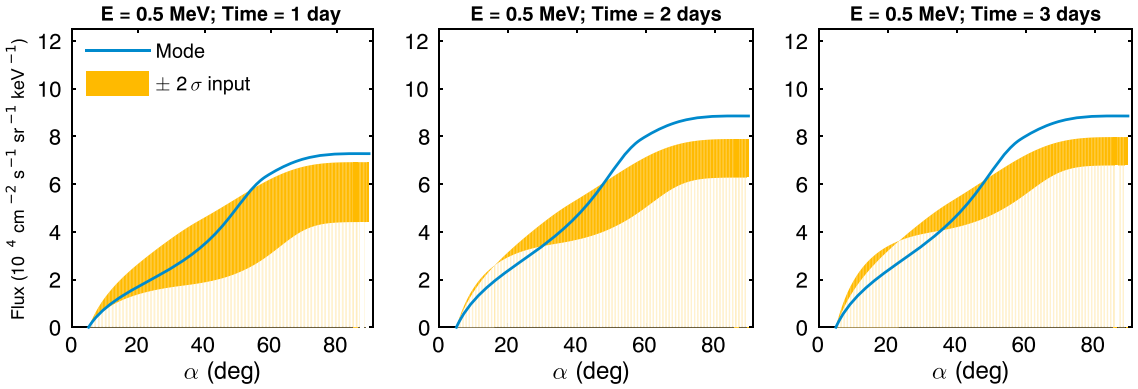

Figure 9. Sensitivity study varying only λ_{max}. Electron flux (in 10^4 cm^{-2} s^{-1} sr^{-1} keV^{-1}) as a function of pitch angle α for energy equal to 500 keV. (left, middle, and right) The evolution at times 1, 2, and 3 days. The blue line is the single simulation corresponding to the most probable inputs. The yellow area denotes the extreme values considered in the input distribution ($\pm 2\sigma$).

the asymmetry of the distribution is clear. In particular, for 60° and 80° pitch angles, the distribution of fluxes is quite broad, being almost constant across 2 orders of magnitude. In this circumstance, a forecast based on a single simulation should certainly carry a large error bar.

3.1. Dependency on a Single Parameter

We can now estimate the relative importance between the three parameters under consideration in determining the variance of the output flux discussed in Figures 3 and 4. This can easily be done by selecting in our ensemble of simulations the ones where only one parameter at a time changes, and the other two are kept fixed at their most probable value (that is, $Kp = 6$, $\lambda_{max} = 35$ (day), 15 (night), and $n = 23.5$ (day), 15.8 (night)). One has to keep in mind that an important simplifying assumption in our methodology is that the three input parameters are independent. This might not be the case in reality, and the resulting conditional distributions might yield smaller variances than the one considered here.

The effect of a change in the maximum value reached by *Kp* during the storm is shown in Figures 7 and 8, for 500 keV and 2 MeV, respectively. Here and in the following figures, the blue line shows the simulation corresponding to the mode of the input distribution (the red dashed lines of the previous figures). Because we are now looking at five simulations only, it does not make sense to compute a cumulative distribution function. Instead, we show as the upper and lower bounds of a yellow area the results of the simulations corresponding to the largest and smallest values of *Kp*, that is, 2 standard deviations apart from the mean. It is interesting to notice how the variance in the flux shrinks, moving from day 1 to day 3 for 500 keV electrons, while it increases for 2 MeV. This might suggest a saturation of the wave energy available to resonate with 500 keV electrons. Yet the largest variation in the results (Figure 8, right) is several times smaller than the

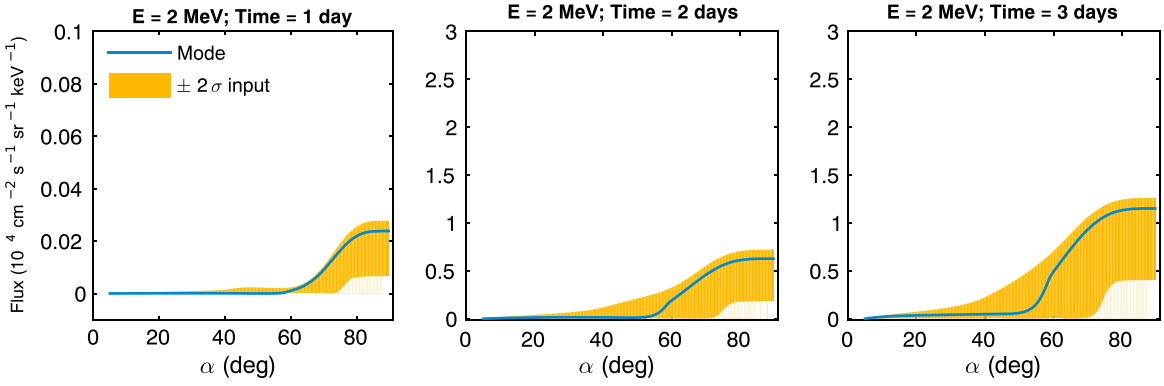

Figure 10. Sensitivity study varying only λ_{max}. Electron flux (in 10^4 cm^{-2} s^{-1} sr^{-1} keV^{-1}) as a function of pitch angle α for energy equal to 2 MeV. (left, middle, and right) The evolution at times 1, 2, and 3 days. The blue line is the single simulation corresponding to the most probable inputs. The yellow area denotes the extreme values considered in the input distribution ($\pm 2\sigma$).

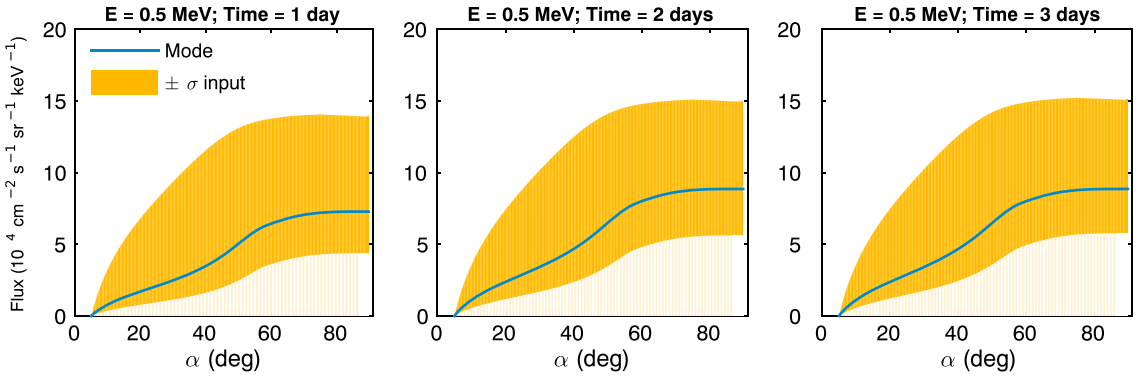

Figure 11. Sensitivity study varying only density. Electron flux (in 10^4 cm^{-2} s^{-1} sr^{-1} keV^{-1}) as a function of pitch angle α for energy equal to 500 keV. (left, middle, and right) The evolution at times 1, 2, and 3 days. The blue line is the single simulation corresponding to the most probable inputs. The yellow area denotes the extreme values considered in the input distribution ($\pm\sigma$).

overall variation observed in Figure 4. Hence, we deduce that variations in *Kp* do not play a major role in the flux variance. With a similar format, we show in Figures 9 and 10 the results concerning the variation of λ_{max} only. Here the nonlinearity of the simulations manifests explicitly in Figure 9 (middle and right). Increasing the value of λ_{max} does not necessarily result in a larger flux, and indeed the curves that bound the yellow region intersect and the blue line (that corresponds to a value of λ_{max} between the $\pm 2\sigma$ extrema) is outside of the yellow region. Also, in this case the variances are much smaller than the one calculated from the whole ensemble (Figures 3 and 4). Consequently, one deduces that most of the variance should be due to variations of the electron density. This is confirmed by looking at the results generated by varying the density only, shown in Figures 11 and 12 for 500 keV and 2 MeV, respectively. The dashed yellow areas are now much larger and comparable to the variance reported for the whole ensemble (we note that the yellow areas in Figures 11 and 12 do not have the same meaning as the ones in Figures 3 and 4).

3.2. Coefficient of Variation

The electron flux in the domain under consideration can vary by a few orders of magnitude. In this case the standard deviation is not very informative. A better measure to define the spread in the ensemble distribution is given by the coefficient of variation, which is defined as the adimensional ratio between the standard deviation and the mean. This is shown in Figure 13 over the whole two-dimensional grid, in logarithmic scale (left, middle, and right are for days 1, 2, and 3). By definition, by virtue of the boundary condition, this quantity is zero at the low energy boundary. One can appreciate that the coefficient of variation increases with larger energies, and it has a much stronger dependence on energy than on pitch angle. Above 1 MeV, this quantity can reach values as large as 10 or 100, indicating a large spread in the distributions, consistent with the histograms shown in Figures 5 and 6.

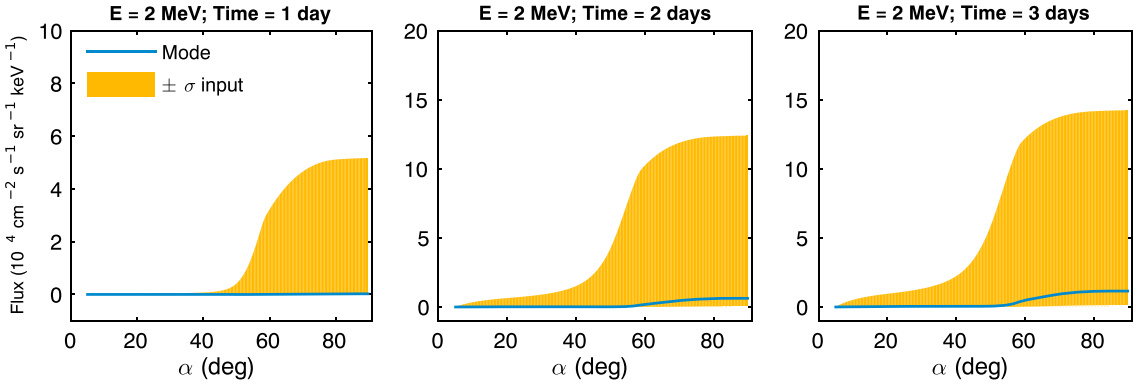

Figure 12. Sensitivity study varying only density. Electron flux (in 10^4 cm^{-2} s^{-1} sr^{-1} keV^{-1}) as a function of pitch angle α for energy equal to 2 MeV. (left, middle, and right) The evolution at times 1, 2, and 3 days. The blue line is the single simulation corresponding to the most probable inputs. The yellow area denotes the extreme values considered in the input distribution ($\pm\sigma$).

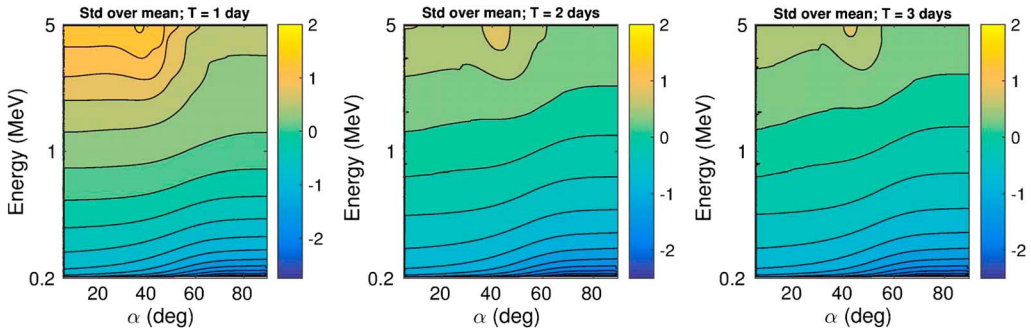

Figure 13. Coefficient of variation: ratio of the standard deviation over the mean of the flux, over the two-dimensional simulation domain (energy, pitch angle). (left, middle, and right) Days 1, 2, and 3. The colorbar is in logarithmic scale.

4. Conclusions

We have reported the first study that addresses the problem of the propagation of uncertainties through quasi-linear diffusion simulations, in the Earth's radiation belt. In this paper, among the many input parameters that one could choose, we have restricted our focus on three parameters only: the maximum value of the geomagnetic index *Kp* during the main phase of a storm, the maximum latitudinal extent of the waves λ_{max}, and the average electron density *n*. Moreover, we have only included parallel-propagating chorus day and night waves and studied diffusion in energy and pitch angle space, at constant $L^* = 4.5$. Once again, we remind the reader that the assumption of statistical independence between the three input parameters constitutes a simplifying and ideal case, which should be refined in future studies. We have employed an ensemble technique, where 225 simulations were performed, each one with a different choice of input parameters and a different assigned probability. For simplicity, the input parameter space has been assumed distributed according to a multivariate Gaussian. The main results of this paper can be summarized as follows:

1. Most of the variance can be attributed to the uncertainty in the density distribution. Note that among the three inputs, the density is the one that has been modeled less arbitrarily. Indeed, it follows the distribution derived in *Sheeley et al.* [2001] from the statistical analysis of CRRES data. This model has been extensively used in several simulations [see, e.g., *Horne et al.*, 2005; *Thorne et al.*, 2005; *Li et al.*, 2007; *Ni et al.*, 2008; *Shprits et al.*, 2008; *Thorne et al.*, 2013].
2. The histograms of the flux are skewed, suggesting an important role of nonlinearities in mapping a Gaussian distribution of inputs into a non-Gaussian distribution of flux. This result suggests using some caution in future studies, where a higher-dimensional input space would require the use of more sophisticated techniques. For instance, stochastic collocation methods involve some form of interpolation that might rapidly degrade the accuracy of the results when not enough collocation points are used.
3. The simulated flux for 2 MeV electrons presents, for large pitch angles, a wide distribution with almost constant probability, ranging about 2 orders of magnitude. Consequently, predictions based on this model should carry large error bars.
4. The coefficient of variation, defined as the standard deviation divided by the mean, calculated on the fluxes presents a much stronger dependence on the energy than on the pitch angle.

In conclusion, this work emphasizes the need to shift to a probabilistic interpretation of the results of physics-based models. The majority of radiation belt models are deterministic. However, we have shown how single-point estimates can be misleading if used as a forecast and if not accompanied by a quantification of the uncertainties involved. In particular, for MeV electrons, we have discussed how the distribution of fluxes can yield results that are 1 or 2 orders of magnitude off from the single simulation performed with the most probable input values. Future extensions of this work will include cross-term diffusion, oblique wave propagation, and radial diffusion. Finally, we suggest that the reduction of the variance in the estimation of the average electron density in the radiation belts should be an important and urgent research goal for the near future [*Sicard-Piet et al.*, 2014; *Zhelavskaya et al.*, 2016], especially in light of the large amount of data recently collected by Van Allen Probes.

Acknowledgments
All the simulation data used in this paper can be requested from the corresponding author. Simon Wing acknowledges support from NSF grant AGS-1058456 and NASA grants (NNX13AE12G, NNX15AJ01G, and NNX16AC39G).

References

Agapitov, O., A. Artemyev, V. Krasnoselskikh, Y. V. Khotyaintsev, D. Mourenas, H. Breuillard, M. Balikhin, and G. Rolland (2013), Statistics of whistler mode waves in the outer radiation belt: Cluster STAFF-SA measurements, *J. Geophys. Res. Space Physics*, *118*, 3407–3420, doi:10.1002/jgra.50312.

Albert, J. (2013), Comment on "On the numerical simulation of particle dynamics in the radiation belt. Part I: Implicit and semi-implicit schemes" and "On the numerical simulation of particle dynamics in the radiation belt. Part II: Procedure based on the diagonalization of the diffusion tensor" by E. Camporeale et al., *J. Geophys. Res. Space Physics*, *118*, 7762–7764, doi:10.1002/2013JA019126.

Albert, J., and S. Young (2005), Multidimensional quasi-linear diffusion of radiation belt electrons, *Geophys. Res. Lett.*, *32*, L14110, doi:10.1029/2005GL023191.

Albert, J. M., M. J. Starks, R. B. Horne, N. P. Meredith, and S. A. Glauert (2016), Quasi-linear simulations of inner radiation belt electron pitch angle and energy distributions, *Geophys. Res. Lett.*, *43*, 2381–2388, doi:10.1002/2016GL067938.

Bourdarie, S., and V. Maget (2012), Electron radiation belt data assimilation with an ensemble Kalman filter relying on the Salammbô code, *Ann. Geophys.*, *30*, 929–943, Copernicus GmbH.

Bourdarie, S., D. Boscher, T. Beutier, J.-A. Sauvaud, and M. Blanc (1996), Magnetic storm modeling in the Earth's electron belt by the Salammbô code, *J. Geophys. Res.*, *101*(A12), 27,171–27,176.

Camporeale, E. (2015), Resonant and nonresonant whistlers-particle interaction in the radiation belts, *Geophys. Res. Lett.*, *42*, 3114–3121, doi:10.1002/2015GL063874.

Camporeale, E., and G. Zimbardo (2015), Wave-particle interactions with parallel whistler waves: Nonlinear and time-dependent effects revealed by particle-in-cell simulations, *Phys. Plasmas*, *22*(9), 092104.

Camporeale, E., G. Delzanno, S. Zaharia, and J. Koller (2013a), On the numerical simulation of particle dynamics in the radiation belt: 1. Implicit and semi-implicit schemes, *J. Geophys. Res. Space Physics*, *118*, 3463–3475, doi:10.1002/jgra.50293.

Camporeale, E., G. Delzanno, S. Zaharia, and J. Koller (2013b), On the numerical simulation of particle dynamics in the radiation belt: 2. Procedure based on the diagonalization of the diffusion tensor, *J. Geophys. Res. Space Physics*, *118*, 3476–3484, doi:10.1002/jgra.50278.

Camporeale, E., G. Delzanno, S. Zaharia, and J. Koller (2013c), Reply to comment by J.M. Albert on "on the numerical simulation of particle dynamics in the radiation belt. Part I: Implicit and semi-implicit scheme" and"on the numerical simulation of particle dynamics in the radiation belt. Part II: Procedure based on the diagonalization of the diffusion tensor", *J. Geophys. Res. Space Physics*, *118*, 7765–7767, doi:10.1002/2013JA019389.

Gallagher, D. L., P. D. Craven, and R. H. Comfort (2000), Global core plasma model, *J. Geophys. Res.*, *105*(A8), 18–819.

Glauert, S. A., R. B. Horne, and N. P. Meredith (2014), Three-dimensional electron radiation belt simulations using the BAS radiation belt model with new diffusion models for chorus, plasmaspheric hiss, and lightning-generated whistlers, *J. Geophys. Res. Space Physics*, *119*, 268–289, doi:10.1002/2013JA019281.

Horne, R., S. Glauert, N. Meredith, D. Boscher, V. Maget, D. Heynderickx, and D. Pitchford (2013), Space weather impacts on satellites and forecasting the Earth's electron radiation belts with SPACECAST, *Space Weather*, *11*, 169–186, doi:10.1002/swe.20023.

Horne, R. B., et al. (2005), Wave acceleration of electrons in the Van Allen radiation belts, *Nature*, *437*(7056), 227–230.

Huang, X., B. W. Reinisch, P. Song, J. L. Green, and D. L. Gallagher (2004), Developing an empirical density model of the plasmasphere using IMAGE/RPI observations, *Adv. Space Res.*, *33*(6), 829–832.

Jaynes, A., et al. (2015), Source and seed populations for relativistic electrons: Their roles in radiation belt changes, *J. Geophys. Res. Space Physics*, *120*, 7240–7254, doi:10.1002/2015JA021234.

Kennel, C., and F. Engelmann (1966), Velocity space diffusion from weak plasma turbulence in a magnetic field, *Phys.Fluids*, *9*(12), 2377–2388.

Knipp, D. J. (2016), Advances in space weather ensemble forecasting, *Space Weather*, *14*, 52–53, doi:10.1002/2016SW001366.

L'Ecuyer, P., and A. B. Owen (2009), *Monte Carlo and Quasi-Monte Carlo Methods 2008*, Springer, Berlin.

Lemons, D. S. (2012), Pitch angle scattering of relativistic electrons from stationary magnetic waves: Continuous Markov process and quasilinear theory, *Phys. Plasmas*, *19*(1), 012306.

Li, W., Y. Shprits, and R. Thorne (2007), Dynamic evolution of energetic outer zone electrons due to wave-particle interactions during storms, *J. Geophys. Res.*, *112*, A10220, doi:10.1029/2007JA012368.

Ma, Q., et al. (2015), Modeling inward diffusion and slow decay of energetic electrons in the Earth's outer radiation belt, *Geophys. Res. Lett.*, *42*, 987–995, doi:10.1002/2014GL062977.

Meredith, N. P., R. M. Thorne, R. B. Horne, D. Summers, B. J. Fraser, and R. R. Anderson (2003), Statistical analysis of relativistic electron energies for cyclotron resonance with EMIC waves observed on CRRES, *J. Geophys. Res.*, *108*(A6), 1250, doi:10.1029/2002JA009700.

Meredith, N. P., R. B. Horne, T. Kersten, B. J. Fraser, and R. S. Grew (2014), Global morphology and spectral properties of EMIC waves derived from CRRES observations, *J. Geophys. Res. Space Physics*, *119*, 5328–5342, doi:10.1002/2014JA020064.

Ni, B., R. M. Thorne, Y. Y. Shprits, and J. Bortnik (2008), Resonant scattering of plasma sheet electrons by whistler-mode chorus: Contribution to diffuse auroral precipitation, *Geophys. Res. Lett.*, *35*, L11106, doi:10.1029/2008GL034032.

Ragot, B. (2012), Pitch-angle scattering: Resonance versus nonresonance, a basic test of the quasilinear diffusive result, *Astrophys. J.*, *744*(1), 75.

Schunk, R., et al. (2016), Space weather forecasting with a multimodel ensemble prediction system (MEPS), *Radio Sci.*, *51*, 1157–1165, doi:10.1002/2015RS005888.

Shalchi, A., and R. Schlickeiser (2005), Evidence for the nonlinear transport of galactic cosmic rays, *Astrophys. J. Lett.*, *626*(2), L97.

Sheeley, B., M. Moldwin, H. Rassoul, and R. Anderson (2001), An empirical plasmasphere and trough density model: CRRES observations, *J. Geophys. Res.*, *106*(A11), 25,631–25,641.

Shprits, Y. Y., N. P. Meredith, and R. M. Thorne (2007), Parameterization of radiation belt electron loss timescales due to interactions with chorus waves, *Geophys. Res. Lett.*, *34*, L11110, doi:10.1029/2006GL029050.

Shprits, Y. Y., D. A. Subbotin, N. P. Meredith, and S. R. Elkington (2008), Review of modeling of losses and sources of relativistic electrons in the outer radiation belt II: Local acceleration and loss, *J. Atmos. Sol. Terr. Phys.*, *70*(14), 1694–1713.

Shprits, Y. Y., D. Subbotin, and B. Ni (2009), Evolution of electron fluxes in the outer radiation belt computed with the verb code, *J. Geophys. Res.*, *114*, A11209, doi:10.1029/2008JA013784.

Sicard-Piet, A., D. Boscher, R. Horne, N. Meredith, and V. Maget (2014), Effect of plasma density on diffusion rates due to wave particle interactions with chorus and plasmaspheric hiss: Extreme event analysis, *Ann. Geophys.*, *32*, 1059–1071, Copernicus Publications on behalf of the European Geosciences Union.

Smith, R. C. (2013), *Uncertainty Quantification: Theory, Implementation, and Applications*, vol. 12, SIAM, Philadelphia, Pa.

Su, Z., F. Xiao, H. Zheng, and S. Wang (2010), STEERB: A three-dimensional code for storm-time evolution of electron radiation belt, *J. Geophys. Res.*, *115*, A09208, doi:10.1029/2009JA015210.

Subbotin, D. A., and Y. Y. Shprits (2009), Three-dimensional modeling of the radiation belts using the Versatile Electron Radiation Belt (VERB) code, *Space Weather*, *7*, S10001, doi:10.1029/2008SW000452.

Subbotin, D. A., and Y. Y. Shprits (2012), Three-dimensional radiation belt simulations in terms of adiabatic invariants using a single numerical grid, *J. Geophys. Res.*, *117*, A05205, doi:10.1029/2011JA017467.

Tao, X., L. Zhang, C. Wang, X. Li, J. Albert, and A. Chan (2016), An efficient and positivity-preserving layer method for modeling radiation belt diffusion processes, *J. Geophys. Res. Space Physics*, *121*, 305–320, doi:10.1002/2015JA022064.

Thorne, R., et al. (2013), Rapid local acceleration of relativistic radiation-belt electrons by magnetospheric chorus, *Nature*, *504*(7480), 411–414.

Thorne, R. M. (2010), Radiation belt dynamics: The importance of wave-particle interactions, *Geophys. Res. Lett.*, *37*, L22107, doi:10.1029/2010GL044990.

Thorne, R. M., T. O'Brien, Y. Shprits, D. Summers, and R. B. Horne (2005), Timescale for MeV electron microburst loss during geomagnetic storms, *J. Geophys. Res.*, *110*, A09202, doi:10.1029/2004JA010882.

Tóth, G., et al. (2012), Adaptive numerical algorithms in space weather modeling, *J. Comput. Phys.*, *231*(3), 870–903.

Tu, W., G. Cunningham, Y. Chen, M. Henderson, E. Camporeale, and G. Reeves (2013), Modeling radiation belt electron dynamics during GEM challenge intervals with the DREAM3D diffusion model, *J. Geophys. Res. Space Physics*, *118*, 6197–6211, doi:10.1002/jgra.50560.

Tu, W., G. Cunningham, Y. Chen, S. Morley, G. Reeves, J. Blake, D. Baker, and H. Spence (2014), Event-specific chorus wave and electron seed population models in DREAM3D using the Van Allen Probes, *Geophys. Res. Lett.*, *41*, 1359–1366, doi:10.1002/2013GL058819.

Xiao, F., Z. Su, H. Zheng, and S. Wang (2009), Modeling of outer radiation belt electrons by multidimensional diffusion process, *J. Geophys. Res.*, *114*, A03201, doi:10.1029/2008JA013580.

Xiao, F., Z. Su, H. Zheng, and S. Wang (2010), Three-dimensional simulations of outer radiation belt electron dynamics including cross-diffusion terms, *J. Geophys. Res.*, *115*, A05216, doi:10.1029/2009JA014541.

Xiao, F., et al. (2014), Chorus acceleration of radiation belt relativistic electrons during March 2013 geomagnetic storm, *J. Geophys. Res. Space Physics*, *119*(5), 3325–3332, doi:10.1002/2014JA019822.

Xiu, D. (2009), Fast numerical methods for stochastic computations: A review, *Commun. Comput. Phys.*, *5*(2–4), 242–272.

Zhelavskaya, I., M. Spasojevic, Y. Shprits, and W. Kurth (2016), Automated determination of electron density from electric field measurements on the Van Allen Probes spacecraft, *J. Geophys. Res. Space Physics*, *121*, 4611–4625, doi:10.1002/2015JA022132.

Zheng, L., A. A. Chan, J. M. Albert, S. R. Elkington, J. Koller, R. B. Horne, S. A. Glauert, and N. P. Meredith (2014), Three-dimensional stochastic modeling of radiation belts in adiabatic invariant coordinates, *J. Geophys. Res. Space Physics*, *119*, 7615–7635, doi:10.1002/2014JA020127.